# Kinetic study on self-energy and stopping power of charged particles moving in metallic carbon nanotubes

Yuan-Hong Song, Dan Zhao, and You-Nian Wang*

*State Key Laboratory of Materials Modification by Beams, School of Physics and Optoelectronic Technology, Dalian University of Technology, Dalian 116024, People's Republic of China*

(Received 7 April 2008; published 14 July 2008)

A semiclassical kinetic model is developed to simulate the plasmon excitation of nanotubes and the transport of charged particles moving through nanotubes. With the introduction of electron band structure, the analytical expressions of the dielectric function and the energy loss function are obtained for zigzag and armchair nanotubes of metallic properties, respectively. Numerical results display several very distinct peaks in the curves of loss function, showing effects from the collective excitation. Furthermore, the stopping power and self-energy are calculated while charged particles move along the axis of nanotubes with different geometries, under the influence of friction coefficients. For small enough friction coefficients, it can be regarded as a case with zero damping. But as the damping factor increases, not only the self-energy and stopping power decrease in magnitude, but also their extrema move to lower velocities, without distinct threshold effects.

DOI: 10.1103/PhysRevA.78.012901 PACS number(s): 61.85.+p, 73.63.−b, 73.20.Mf

## I. INTRODUCTION

Going with the discovery of carbon nanotubes by Iijima in 1991 [1], much attention has been paid to the theoretical and experimental researches in various aspects due to the remarkable physical characters and applied values. The single-walled nanotube (SWNT), as a hollow structure rolled by a graphitic carbon plane, offers an interesting alternative for channeled particles, in a manner similar to the crystal channeling. As an aligned array of straight parallel nanotubes, multiwalled nanotubes (MWNTs) can be also treated as a subject of channeling research, with the spacing narrower than the width of SWNT but still larger than the spacing in the crystal lattice channels. Theoretical investigations were developed by several authors [2–5], focusing on the transport of fast charged particles through carbon nanotubes. It was found that, compared with the traditional crystal channels, carbon nanotubes can obtain wider channels in two dimensions and longer dechanneling lengths owing to a very low electron density in their interior. As for the experimental progresses, it is noted that the transport of electrons with kinetic energies of 300 keV through single and well aligned carbon nanotubes has been achieved recently in experiments [6]. Besides, the experiment for 2 MeV $He^+$ ions channeling in carbon nanotubes has been realized for the first time [7], encouraging more theoretical researchers to investigate nanotubes as channeling and focusing elements.

While channeling through the hollow region of the nanotubes, one of the most concerning problems is the electronic excitations of the nanotube surface. In experiments, the excitation of the surface plasmon was discussed by the characteristic energy-loss curves of the reflected electrons transmitted through the cylindric microchannels [8]. From the discovery of nanotubes, collective excitations of valence electrons in nanotubes have been probed also from the measurement of loss function in the EELS (electron energy-loss spectroscopy) [9,10].

Besides, important achievements have been made in the aspect of theoretical researches. Including the quantum effects, random-phase approximation (RPA) in the dielectric response theory has been used as a valid tool to discuss the elementary excitation of the quasi-one-dimensional tubule system [11,12]. Also by means of the dielectric theory, Arista has studied the channeling of fast ions and clusters through microcapillaries and nanocapillaries in solids, setting their pioneering work on the surface excitation mode, induced potential, energy loss, and self-energy [13–15]. Furthermore, the energy loss of charged particles moving parallel to the axis in cylindrical tubules is calculated by using the same theory while taking the tubules as an infinitesimally thin layer of free electron gas [16]. And comparison of the stopping power from plasmons and single-particle excitations for nanotubes has also been put forward [17]. As a prominent tool to investigate the electronic excitation properties in restricted geometries, the hydrodynamic model is adopted to study the dielectric properties of the carbon nanotubes [18]. Introducing the single-electron excitation term in the two-dimensional fluid model, the self-energy and the energy loss of the charged particles tracking parallel to the axis of a single-walled or a two-walled nanotube have been calculated [19–21]. Moreover, treating the $\sigma$ and $\pi$ electrons as separate two-dimensional fluids constrained to the same cylindrical surface, two-fluid models have been proposed to describe the collective electron excitation in single-walled or multiwalled carbon nanotubes [22,23]. And, the dynamic polarization effects and Coulomb explosions for protons and molecular ions channeling through SWNTs are also investigated in the same hydrodynamic formulation [24,25]. Nevertheless, we have noticed from the above works that, in either the RPA dielectric theory or the hydrodynamic theory, the electron gas of the nanotube surface is considered as a quasi-free-electron gas distributed uniformly over the wall, without any effects of the energy band structure to be taken into account.

As we all know, while considering the layer of the carbon nanotube is infinitesimally thin in comparison with its radius, the structure of nanotubes are defined by a two-dimensional

*ynwang@dlut.edu.cn

 

(2D) lattice vector $R=n\mathbf{a}_1+l\mathbf{a}_2$, where $n$ and $l$ are integers representing the vector characterizing the pattern of rolling a planar sheet to a cylindrical cavity, and $|\mathbf{a}_1|=|\mathbf{a}_2|=2.46$ Å is the lattice constant of a graphite sheet. According to the dual index $(n,l)$, the nanotubes can be classified into zigzag ($l=0$), armchair ($n=l$), and chiral nanotube ($0<n\neq l$), exhibiting either metallic or semiconducting properties. For example, a zigzag nanotube is metallic for $n=3j$ ($j$ is an integer) while an armchair nanotube always behaves like a metal for any $n$. Thus the energy band structure of the electrons on the nanotube surface, in charge of defining the difference between metallic and semiconducting properties, may not be neglected. But, neither the dielectric theory nor the hydrodynamic theory can be valid enough for the investigations of electron excitation and channeling in nanotubes. Much attention may be shed on the work including the band structure effect. Considering the band structure of the electron energy in the formulation of the quantum dielectric theory, Lin and his colleagues have investigated the low-frequency electronic excitations in various carbon nanotubes [26–29]. Moreover, a kinetic theory as well as the classical electrodynamics have been proposed by Slepyan *et al.* [30] to describe the electromagnetic processes in carbon nanotubes [31,32]. In this paper, the semiclassical Boltzmann kinetic equation is adopted in the framework of momentum-independent relaxation time approximation, trying to put forward a relatively convenient way to investigate the electron excitation of nanotubes under the channeling of the charged particles for different band structure of the electrons.

We will extend the semiclassical kinetic theory [32] to study the collective excitation in nanotubes, with charged particles moving inside the SWNTs and parallel with their axes. The theoretical model will depend on the geometric structures, including the radius and the chiral angle of the nanotube. The self-energy and the stopping power of charged particles are also concerned. Our particular attention will be focused on metallic nanotubes for both zigzag and armchair nanotubes. The calculation details of the dielectric function, the self-energy, and the stopping power function are given in Sec. II. We will discuss the calculation results in Sec. III. Section IV provides brief concluding remarks. We use the cylindrical coordinate system $\mathbf{r}=(\rho,\phi,z)$ for the two kinds of nanotubes, with the orientation of $z$ parallel to the axis of nanotube. Unless otherwise indicated, atomic units (a.u.), where $m_e=\hbar=e=1$, will be used throughout this paper.

## II. THEORETICAL MODEL

Both zigzag nanotubes $(n,l=0)$ and armchair nanotubes $(n,l=n)$ are regarded as infinitesimally thin and infinitely long cylindrical cavities. The radius $a$ of a nanotube is connected to $l$ and $n$ in the form of $a=\frac{b\sqrt{3(l^2+ln+n^2)}}{2\pi}$, where $b=1.44$ Å is the length of the C-C bond of the surface of the nanotube. The electrons of the nanotube surface are assumed to meet the Fermi equilibrium distribution function, with the chemical potential of graphite being null valued [32],

$$f_0(\mathbf{p})=\frac{1}{1+\exp\{\varepsilon(\mathbf{p})/k_BT\}}, \tag{1}$$

where $\varepsilon=\varepsilon(\mathbf{p})$ is the electron energy with respect to Fermi level, $k_B$ is the Boltzmann constant, $T$ is the temperature which remains at 273 K here, and $\mathbf{p}$ is the electron's two-dimensional quasimomentum tangential to the nanotube's surface. In this paper, we only take $\pi$ electrons as our aim for their important effects on electronic properties. By using the tight-binding model, the energy dispersion relations for zigzag and armchair nanotubes can be given as [32–34]

$$\varepsilon(\mathbf{p})=\pm\gamma_0\sqrt{1+4\cos\left(\frac{3bp_z}{2\hbar}\right)\cos\left(\frac{\sqrt{3}bp_\phi}{2\hbar}\right)+4\cos^2\left(\frac{\sqrt{3}bp_\phi}{2\hbar}\right)}\quad \text{for zigzag}(n,0), \tag{2}$$

$$\varepsilon(\mathbf{p})=\pm\gamma_0\sqrt{1+4\cos\left(\frac{3bp_\phi}{2\hbar}\right)\cos\left(\frac{\sqrt{3}bp_z}{2\hbar}\right)+4\cos^2\left(\frac{\sqrt{3}bp_z}{2\hbar}\right)}\quad \text{for armchair}(n,n), \tag{3}$$

where $p_z$ and $p_\phi$ are the projections of $\mathbf{p}$ on the axis and the $\phi$ direction of the nanotube, $\gamma_0=3.033$ eV is the interaction energy for the nearest-neighbor carbon atoms. The sign $\pm$ corresponds to the conduction and valence electrons, respectively. Different from the graphene plane, carbon nanotubes have a structure with a long fiber axis and a circumference of atomic dimensions. So, while the number of allowed states in the axial direction is large, the number of states in the circumferential direction is limited, resulting in the discrete values of the momentum $p_\phi$. Using the periodic boundary condition, the allowed values for $p_\phi$ can be

$$p_\phi=\frac{2\pi\hbar s}{\sqrt{3}nb}s=1,2,\ldots,n\quad \text{for zigzag}(n,0), \tag{4}$$

$$p_\phi=\frac{2\pi\hbar s}{3nb}s=1,2,\ldots,n\quad \text{for armchair}(n,n), \tag{5}$$

where $\hbar$ is the Planck constant divided by $2\pi$.

When a charged particle goes through inside the nanotube, the instantaneous position of it is given by $\mathbf{r}_0=(\rho_0,\phi_0,vt)$ in the cylindrical coordination, involving the

velocity of the particle $v$. We employ $\Phi_2$ to express the potential outside the nanotube ($\rho > a$), while the values of the total potential $\Phi_1 = \Phi_0 + \Phi_{ind}$ inside the nanotube ($\rho < a$) may include the potential $\Phi_0$ from the moving charged particle itself and the potential $\Phi_{ind}$ from the charge polarization on the nanotube surface induced by charged particle. Complying with the work in Ref. [19], these potentials could be expanded in terms of Bessel functions as

$$\Phi_0(\mathbf{r},t) = \frac{Q}{|\mathbf{r}-\mathbf{r}_0|} = \frac{Q}{\pi}\sum_{m=-\infty}^{m=\infty}\int_{-\infty}^{+\infty} dk e^{ik(z-vt)+im(\phi-\phi_0)} \times I_m(k\rho_<)K_m(k\rho_>), \tag{6}$$

$$\Phi_{ind}(\mathbf{r},t) = \frac{Q}{\pi}\sum_{m=-\infty}^{m=\infty}\int_{-\infty}^{+\infty} dk e^{ik(z-vt)+im(\phi-\phi_0)} \times I_m(k\rho_0)I_m(k\rho)A_m(k), \tag{7}$$

and

$$\Phi_2(\mathbf{r},t) = \frac{Q}{\pi}\sum_{m=-\infty}^{m=\infty}\int_{-\infty}^{+\infty} dk e^{ik(z-vt)+im(\phi-\phi_0)} \times I_m(k\rho_0)K_m(k\rho)B_m(k), \tag{8}$$

where $k$ is the longitudinal wave number, $m$ is the angular momentum. Also in these above equations, $Q$ is the charge of the particle, $I_m(x)$ and $K_m(x)$ are the first and second kinds of the modified Bessel function, and $\rho_<$ and $\rho_>$ are the smaller or larger of $\rho$ and $\rho_0$.

Furthermore, exposed to the intrusion of charged ions, the distribution function of $\pi$ electrons on the surface of carbon nanotubes is assumed to satisfy the first-order Boltzmann kinetic equation

$$\frac{\partial f_1}{\partial t} + \mathbf{v}\cdot\nabla_s f_1 = e\mathbf{E}\cdot\frac{\partial f_0}{\partial \mathbf{p}} - \gamma f_1, \tag{9}$$

where $\nabla_s = \frac{1}{a}\frac{\partial}{\partial\phi}\hat{\mathbf{e}}_\phi + \frac{\partial}{\partial z}\hat{\mathbf{e}}_z$ is the two-dimensional differential operator along the surface of the nanotube, $\mathbf{E} = -\nabla\Phi$ is the electric field on the surface, and $f_1$ is the perturbation of the distribution function. And, $\gamma$ is the friction coefficient due to electron scattering on the positive charge background, which is introduced to satisfy the nonconservation of the system. In terms of a Fourier expansion, the perturbation part $f_1$ can be expressed as

$$f_1 = \frac{Q}{\pi}\sum_{m=-\infty}^{m=\infty}\int_{-\infty}^{+\infty} dk e^{ik(z-vt)+im(\phi-\phi_0)} f_{1m}(a,\mathbf{p},k,\omega). \tag{10}$$

Combining Eqs. (9) and (10) with Eq. (8) in which $\Phi = \Phi_2(\mathbf{r},t)|_{\rho=a}$, we can obtain

$$f_{1m}(a,\mathbf{p},k,\omega) = \frac{\partial f_0}{\partial\varepsilon}\frac{e\Phi_m[(m/a)v_\phi + kv_z]}{\omega - (m/a)v_\phi - kv_z + i\gamma}, \tag{11}$$

where $\Phi_m = I_m(k\rho_0)K_m(ka)B_m(k)$, $\omega = kv$, and $v_z = \frac{\partial\varepsilon}{\partial p_z}$, respectively. But for $v_\phi$, considering $p_\phi$ a quantized variable given in Eqs. (4) and (5), we thus approximate the partial derivative with finite difference, as $v_\phi = \varepsilon[p_z, p_\phi(s+1)] - \varepsilon[p_z, p_\phi(s)]$.

In order to determine the coefficients $A_m(k)$ and $B_m(k)$, we take into account the following boundary conditions at $\rho = a$: the potential remains continuous at the cylinder,

$$\Phi_1(\mathbf{r},t)|_{\rho=a} = \Phi_2(\mathbf{r},t)|_{\rho=a}, \tag{12}$$

and the radial component of the displacement field at the boundary keeps discontinuous because of the induced density on the surface nanotube $n_1(a,\phi,z,t)$,

$$\frac{\partial\Phi_2}{\partial\rho}(\mathbf{r},t)\bigg|_{\rho=a} - \frac{\partial\Phi_1}{\partial\rho}(\mathbf{r},t)\bigg|_{\rho=a} = 4\pi n_1(a,\phi,z,t). \tag{13}$$

By using the Fourier expansion, the induced density $n_1(\phi,z,t)$ can be expressed as

$$n_1(a,\phi,z,t) = \frac{Q}{\pi}\sum_{m=-\infty}^{m=\infty}\int_{-\infty}^{+\infty} dk e^{ik(z-vt)+im(\phi-\phi_0)} n_{1m}(a,k,\omega), \tag{14}$$

where

$$n_{1m}(a,k,\omega) = \frac{4}{(2\pi\hbar)^2}\int d\mathbf{p} f_{1m}(a,\mathbf{p},k,\omega). \tag{15}$$

Thus, inserting Eqs. (14), (15), and (11) into the boundary condition in Eqs. (12) and (13), the expressions of the coefficients $A_m$ and $B_m$ can be obtained as follows:

$$A_m(k) = \frac{K_m(ka)}{I_m(ka)}[\epsilon^{-1}(k,m,\omega,a) - 1], \tag{16}$$

$$B_m(k) = \epsilon^{-1}(k,m,\omega,a). \tag{17}$$

In Eqs. (16) and (17), $\epsilon(k,m,\omega,a)$ is the dielectric function of the electron gas on the nanotube surface with the form as

$$\epsilon(k,m,\omega,a) = 1 - 4\pi a I_m(ka)K_m(ka)\chi(k,m,\omega,a), \tag{18}$$

where $4\pi a I_m(ka)K_m(ka)$ is the Fourier transform of the electron-electron Coulomb interaction on the surface of nanotube, and $\chi(k,m,\omega,a)$ is the response function, which has different expressions for zigzag and armchair nanotubes in this model:

$$\chi(k,m,\omega,a) = \frac{4}{\pi\hbar}\frac{1}{\sqrt{3}nb}\sum_{s=1}^{n}\int_{-2\pi/3b}^{2\pi/3b} dp_z \frac{\partial f_0}{\partial\varepsilon}\frac{(m/a)v_\phi + kv_z}{(m/a)v_\phi + kv_z - \omega - i\gamma} \quad \text{for zigzag}, \tag{19}$$

$$\chi(k,m,\omega,a) = \frac{4}{\pi\hbar}\frac{1}{3nb}\sum_{s=1}^{n}\int_{-2\pi/\sqrt{3}b}^{2\pi/\sqrt{3}b} dp_z \frac{\partial f_0}{\partial\varepsilon}\frac{(m/a)v_\phi + kv_z}{(m/a)v_\varphi + kv_z - \omega - i\gamma} \quad \text{for armchair.} \tag{20}$$

So, the dielectric function we obtain here is not only related to the longitudinal wave number $k$, the angular momentum $m$, the frequency $\omega$ of the elementary excitation, and the radius of the nanotube, but also the chiral angle of the nanotube which indicates the different energy dispersion relation of electrons in Eqs. (2) and (3).

From the equations given above, the induced potential inside the nanotube can be written as

$$\Phi_{ind}(\mathbf{r},t) = \frac{Q}{\pi}\sum_{m=-\infty}^{m=\infty}\int_{-\infty}^{+\infty} dk e^{ik(z-vt)+im(\varphi-\varphi_0)} I_m(k\rho_0)I_m(k\rho)\frac{K_m(ka)}{I_m(ka)}[\epsilon^{-1}(k,m,\omega,a)-1]. \tag{21}$$

The self-energy and the stopping power for the ion moving inside a carbon nanotube can also be obtained to show how the electrons' polarization act on the ion channeling. The detailed expressions of the self-energy and stopping power are given as

$$E_{self} = \frac{1}{2}Q\Phi_{ind}(\mathbf{r},t)\Big|_{\mathbf{r}=\mathbf{r}_0(t)} = \frac{Q^2}{2\pi}\sum_{m=-\infty}^{m=\infty}\int_{-\infty}^{\infty} dk I_m^2(|k|\rho_0)\frac{K_m(|k|a)}{I_m(|k|a)} \times\{\mathrm{Re}[\epsilon^{-1}(k,m,\omega,a)]-1\}, \tag{22}$$

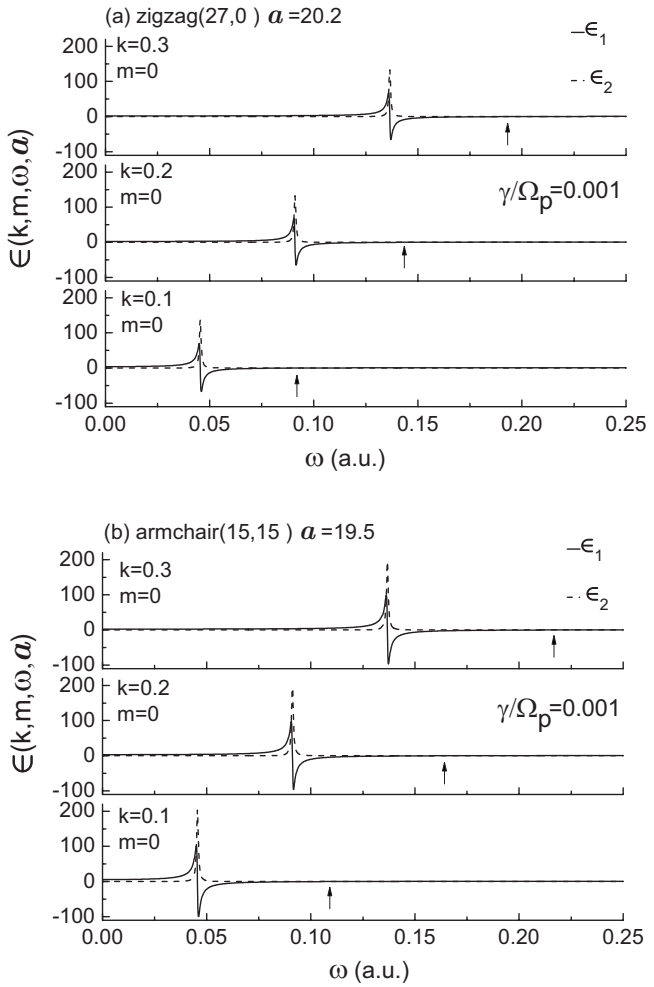


FIG. 1. The dielectric functions dependent on the frequency $\omega$ for (a) zigzag (27, 0) and (b) armchair (15, 15) nanotubes, with $m=0$, $\gamma=0.001\Omega_p$ and different $k=0.1$, 0.2, and 0.3. The real ($\varepsilon_1$) and the imaginary ($\varepsilon_2$) of the dielectric function is shown by the solid and the dash curves, respectively.

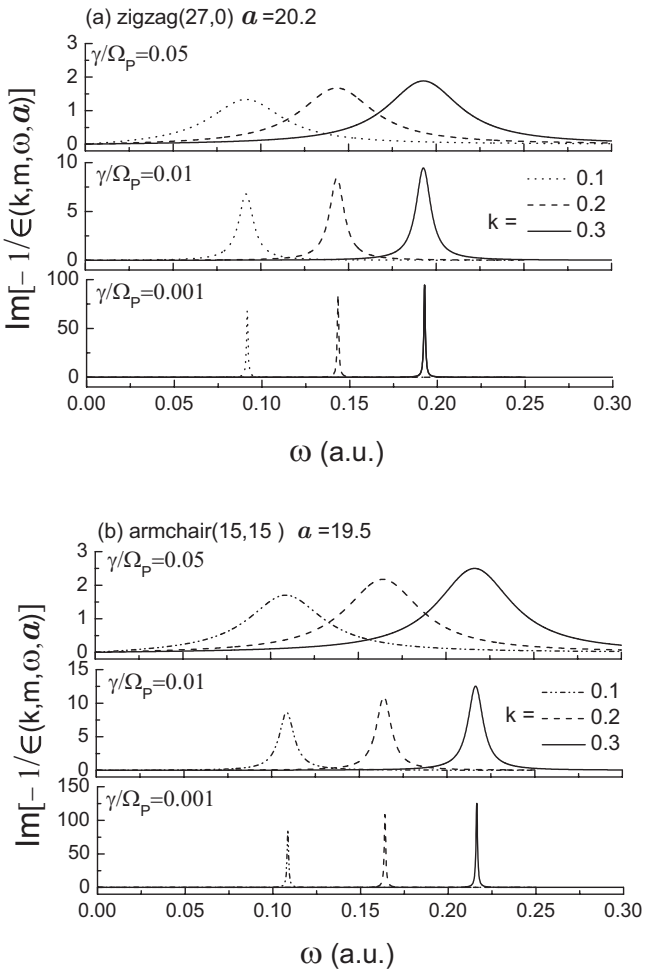


FIG. 2. The loss functions dependent on the frequency $\omega$ for (a) zigzag (27, 0) and (b) armchair (15, 15) nanotubes, with $m=0$, and different $k$ and $\gamma$ values.

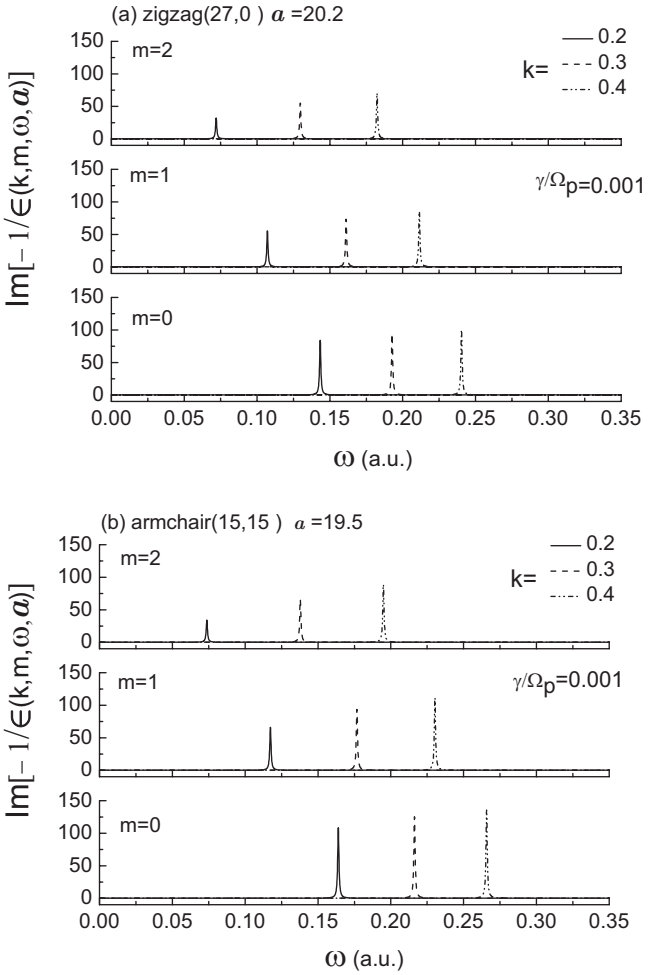


FIG. 3. The loss functions dependent on the frequency $\omega$ for (a) zigzag (27, 0) and (b) armchair (15, 15) nanotubes, with $\gamma = 0.001\Omega_p$, and different $k$ and $m$ values.

$$S = Q\frac{\partial \Phi_{ind}(\mathbf{r},t)}{\partial z}\bigg|_{\mathbf{r}=\mathbf{r}_0(t)} = \frac{Q^2}{\pi}\sum_{m=-\infty}^{m=\infty}\int_{-\infty}^{\infty} dk k I_m^2(|k|\rho_0)\frac{K_m(|k|a)}{I_m(|k|a)}\mathrm{Im}[-\epsilon^{-1}(k,m,\omega,a)]. \tag{23}$$

From Eq. (23), one may notice that the resonant excitations could be figured out in the case that the damping coefficient approaches zero ($\gamma \to 0^+$). As the function $Z_m(k,\omega) = 1 - 4\pi a I_m(ka)K_m(ka)\mathrm{Re}\,\chi(k,m,\omega,a)$ equals zero, the energy loss function $\mathrm{Im}[-\epsilon^{-1}(k,m,\omega,a)]$ in Eq. (23) transforms into a Delta function, leading to

$$S = Q^2\sum_{m=-\infty}^{m=\infty} k_m I_m^2(|k_m|\rho_0)\frac{K_m(|k_m|a)}{I_m(|k_m|a)}\left|\frac{\partial Z_m(k,\omega)}{\partial k}\right|^{-1}_{k=k_m}, \tag{24}$$

where $k_m$ is determined by the condition of the collective resonance $Z_m(k,\omega) = 0$.

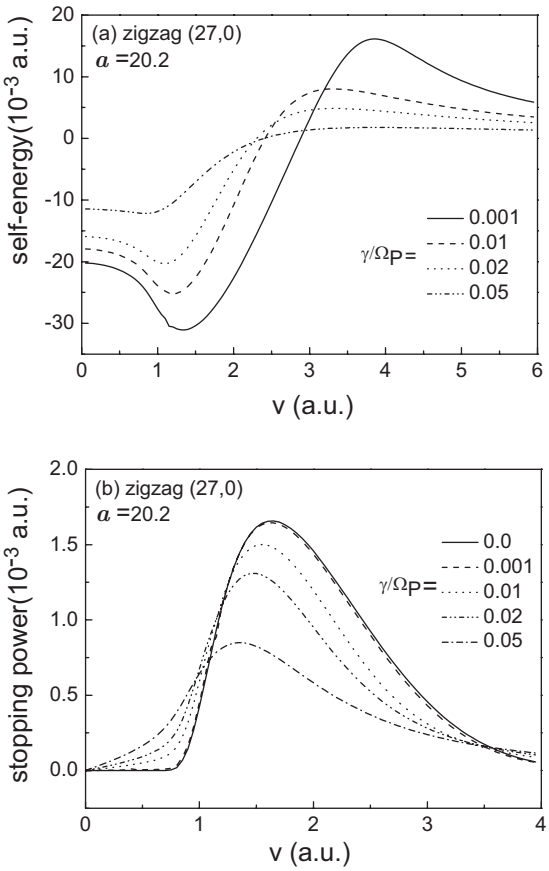


FIG. 4. The dependences of (a) self-energy and (b) stopping power on the proton velocity for zigzag nanotube (27, 0), with different friction coefficient $\gamma$.

## III. RESULTS AND DISCUSSION

The dielectric functions $\epsilon(k,m,\omega,a)$ vs the frequency $\omega$ for (a) zigzag nanotube (27, 0) and (b) armchair nanotube (15, 15) are shown in Fig. 1, with $\gamma = 0.001\Omega_p$, $m = 0$ and three different values of $k$. Here, $\Omega_p = (\frac{4\pi n_0}{a})^{1/2} \approx 0.5$ a.u., $n_0$ is the surface density of the valence electrons, which is obtained from the integration of equilibrium distribution functions $n_0 = \frac{4}{(2\pi\hbar)^2}\int d\mathbf{p} f_0(a,\mathbf{p})$. The real part $\epsilon_1$ and the imaginary part $\epsilon_2$ of the dielectric function are shown by the solid and the dash curves, respectively. One can see from this figure that the curves of $\epsilon_1$ and $\epsilon_2$ exhibit similar shapes which have been presented in Refs. [27,28], in which the theoretical formulation is based on the quantum RPA. Obviously, as the arrows point out in Fig. 1, the trend of $\epsilon_1$ is becoming zero with the increasing of $\omega$, while $\epsilon_2$ approaches zero with the infinitesimally small damping, corresponding to collective excitations on the nanotube surface. Plasmon peaks are also shown in Fig. 2, in which the energy loss function $\mathrm{Im}[-\epsilon^{-1}(k,m,\omega,a)]$ is calculated dependent on the frequency $\omega$ but for different damping $\gamma$. The biggest damping factor adopted here is $\gamma = 0.05\Omega_p \approx 0.68$ eV. It can be observed that the plasmon peaks are damped to become lower and wider for more friction from the atoms. And also, the plasmon excitation tends to occur at higher frequency as the longitudinal wave number $k$ increases. Figure 3 shows the energy

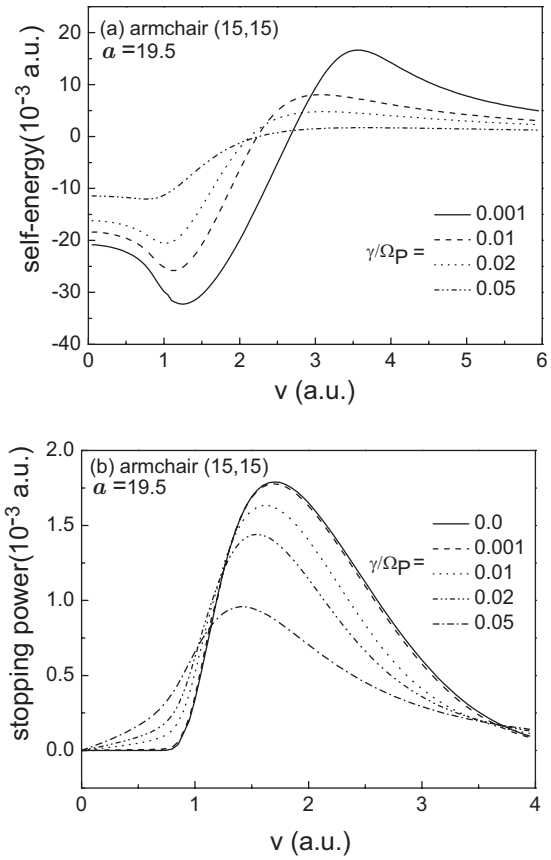


FIG. 5. The dependences of (a) self-energy and (b) stopping power on the proton velocity for armchair nanotube (15, 15), with different friction coefficient $\gamma$.

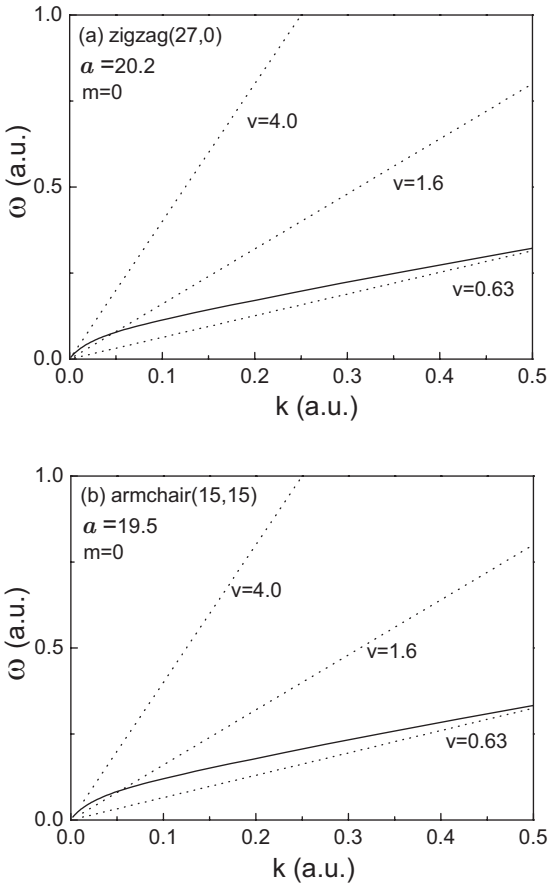


FIG. 6. The dispersion relation from the collective excitation $Z_0(k,\omega)=0$, for (a) the zigzag (27, 0) and (b) armchair (15, 15) nanotubes, respectively. The straight dotted lines correspond to different $v$ for $\omega=kv$.

loss function vs $\omega$ for different angular momentum $m=0$, 1, and 2. As $m$ decreases and $k$ increases, the peak value keeps increasing, suggesting more energy loss, different from the work in Refs. [27,28]. However, considering the asymptotical properties of the modified Bessel function, the term $K_m(|k|a)/I_m(|k|a)$ in Eqs. (23) and (24) approaches zero at a rapid rate as $k$ increases. Thus more contribution will be made to the stopping power in the case of smaller $m$ and $k$ in this theoretical model.

In the following calculations, we will discuss a proton ($Q=1$) moving along the axis of the nanotube ($\rho_0=0$) in zigzag nanotubes and armchair nanotubes, respectively. Thus, on account of axial symmetry, only $m=0$ can be relied on, and the term of $v_\phi$ would be ignored in the expression of the response function in Eq. (11). Considering a set of values of $\gamma$, Figs. 4 and 5 show the effects of the friction coefficient $\gamma$ on (a) the self-energy and (b) stopping power which are functions of the proton's velocity $v$, for zigzag and armchair nanotubes, respectively. Here, the upper limits of the integrals in Eqs. (22) and (23) are cut off at about $k=0.6$ where the integrands are already convergent to zero. As for results of the stopping power in Figs. 4(b) and 5(b), the two curves labeled $\gamma/\Omega_p=0$ are obtained from Eq. (24). As we observe, these two curves come much closer to those labeled $\gamma/\Omega_p=0.001$, showing us a small enough value of the variable $\gamma$ close to the case without damping.

We also notice a sudden increases in the stopping powers at threshold values, for the damping $\gamma/\Omega_p=0$ or 0.001. We plot in Fig. 6 the dispersion relation of resonant excitation spectrum in $k-\omega$ space, obtained from $Z_0(k,\omega)=0$. Considering the expression $\omega=kv$ here, the plasmon mode can only contribute to the stopping power when the straight dotted lines touch the plasmon curve. So, with zero damping, the collective excitation takes place when the proton velocities locate in the range $0.63<v<4.0$, as seen from Fig. 6.

In addition, we could easily see that both the self-energy and the stopping power keep decreasing in magnitude, while the self-energy negative peaks and the stopping power maxima move to lower velocities, with the increasing damping factors, similar to the works given by Refs. [15,16,19]. As the peaks move with the increasing $\gamma$, the threshold behavior for stopping power at low velocities also disappears. So, from Figs. 4(b) and 5(b), with the factor $\gamma$ larger than $0.001\Omega_p$, the stopping can also be noticed for the proton with speed $v<0.63$, showing relaxing effects from damping of the plasmon resonances.

Figures 7 and 8 show the impact of the nanotube chiral parameter $n$ on the self-energy and stopping power, also for zigzag and armchair nanotubes, respectively, with the friction coefficient $\gamma=0.001\Omega_p$ and $\gamma=0.05\Omega_p$. From these two figures one can see that, as the chiral parameter $n$ and the radiuses of nanotubes increase, protons along the axis keep away from the nanotube surface, resulting in the decrease in

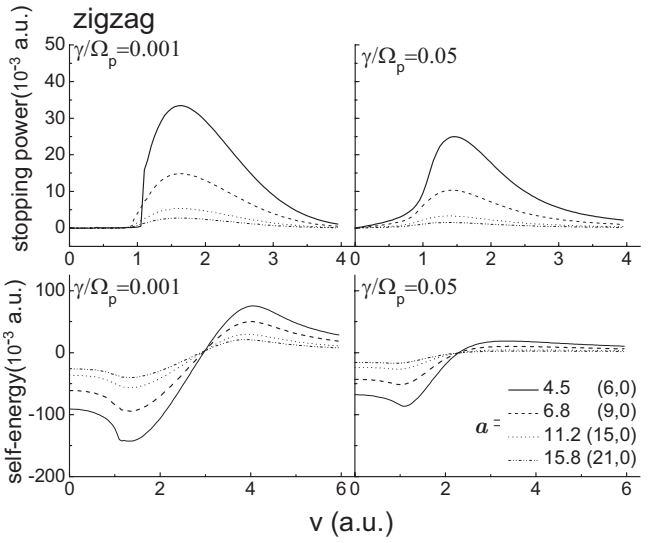


FIG. 7. The dependences of the self-energy and stopping power on the proton velocity for different zigzag nanotubes $(n,0)$, with the friction coefficient $\gamma=0.001\Omega_p$ and $\gamma=0.05\Omega_p$.

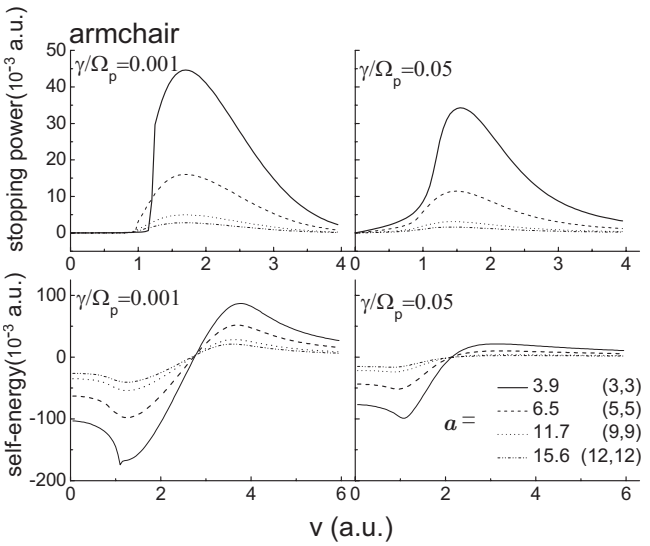


FIG. 8. The dependences of the self-energy and stopping power on the proton velocity for different armchair nanotubes $(n,n)$, with the friction coefficient $\gamma=0.001\Omega_p$ and $\gamma=0.05\Omega_p$.

magnitude of the self-energy and stopping power, similar to the work in Refs. [16,19]. And also, by comparing the cases of different damping values, the increase of gamma brings a decrease of the stopping power and self-energy values and the proton speed thresholds relax, but with almost slight shifts of the extrema position for nanotubes with different radiuses. So more damping is the main reason for the shift of collective excitation to the lower speed region and the indistinctness of the threshold effect.

## IV. CONCLUDING REMARKS

In this work, a theoretical model based on the semiclassical kinetic theory is employed to describe the electron excitation on the surface of the zigzag and armchair nanotubes of metallic character. By adopting the electron dispersion relation of the nanotube, the real band structure of electrons can be embodied to affect the characters of the dielectric function $\epsilon(k,m,\omega,a)$ and the loss function $\mathrm{Im}[-\varepsilon^{-1}(k,m,\omega,a)]$. General expressions of the dielectric function and energy loss function are accordingly derived, which are relative to the radius and chiral angle of the nanotubes. The plasmon excitation, which is dependent on the nanotube geometry, the longitudinal wave number, the angular momentum, and the friction coefficient, can be identified from the dielectric function profiles and the sharp peaks in the loss function.

And then, analytical expressions of the induced potential, the self-energy, and the stopping power are obtained for a charged particle moving paraxially in nanotubes. Here, we focus our attention on the case where protons move along the axis of the nanotubes. The simulation results are shown and indicate strong dependences on the damping factor and the nanotube geometry. As the damping factor $\gamma$ increases, the self-energy and the stopping power keep decreasing in magnitude, and the extrema position of the stopping power move to the lower velocity region, suggesting more damping effects on the collective excitation. The stopping power results also show that the damping $\gamma=0.001\Omega_p$ is small enough to be taken as a case without damping. And in this case, as the radius of the two kinds of nanotube increases, the self-energy and the stopping power decrease in magnitude, but with almost no shifts of the maxima position. However, this maxima position of the stopping power, located at about $v=1.6$, is much different from the works in RPA [16] and hydrodynamics formulations [19]. From our comprehension, aside from the introduction of the electron band structure, the kinetic model which is suitable for both high and low velocity cases is also one of the reasons.

In conclusion, we try to provide a new way of simulating the electron excitation and the stopping power for charged particles moving along the nanotube axes in this paper. The results obtained make us believe that the kinetic model is available and apt for studies of the transport behavior through nanotubes, especially for different nanotube geometries and even for multiwalled nanotubes in future work.

## ACKNOWLEDGMENTS

This work was supported by the National Natural Science Foundation of China (Y.N.W.), Grant No. 10275009.

[1] S. Iijima, Nature (London) **354**, 56 (1991).
[2] V. V. Klimov and V. S. Letokhov, Phys. Lett. A **226**, 244 (1997).
[3] N. K. Zhevago and V. I. Glebov, Phys. Lett. A **250**, 360 (1998).
[4] V. M. Biryukov and S. Bellucci, Phys. Lett. B **542**, 111 (2002).
[5] S. Bellucci, V. M. Biryukov, and A. Cordelli, Phys. Lett. B **608**, 53 (2005).
[6] G. Chai, H. Heinrich, L. Chow, and T. Schenkel, Appl. Phys. Lett. **91**, 103101 (2007).
[7] Z. Zhu, D. Zhu, R. Lu, Z. Xu, W. Zhang, and H. Xia, Proc. SPIE **5974**, 597413 (2005).
[8] K. C. Mamola, R. J. Warmack, and T. L. Ferrell, Phys. Rev. B **35**, 2682 (1987).
[9] T. Pichler, M. Knupfer, M. S. Golden, J. Fink, A. Rinzler, and R. E. Smalley, Phys. Rev. Lett. **80**, 4729 (1998).
[10] M. Knupfer, T. Pichler, M. S. Golden, J. Fink, A. Rinzler, and R. E. Smalley, Carbon **37**, 733 (1999).
[11] O. Sato, Y. Tanaka, M. Kobayashi, and A. Hasegawa, Phys. Rev. B **48**, 1947 (1993).
[12] M. F. Lin and W.-K. Kenneth Shung, Phys. Rev. B **47**, 6617 (1993).
[13] N. R. Arista, Nucl. Instrum. Methods Phys. Res. B **182**, 109 (2001).
[14] N. R. Arista and M. A. Fuentes, Phys. Rev. B **63**, 165401 (2001).
[15] N. R. Arista, Phys. Rev. A **64**, 032901 (2001).
[16] Y. N. Wang and Z. L. Mišković, Phys. Rev. A **66**, 042904 (2002).
[17] G. Gumbs and A. Balassis, Phys. Rev. B **71**, 235410 (2005).
[18] T. Stöckli, J. M. Bonard, A. Châtelain, Z. L. Wang, and P. Stadelmann, Phys. Rev. B **64**, 115424 (2001).
[19] Y. N. Wang and Z. L. Mišković, Phys. Rev. A **69**, 022901 (2004).
[20] D. J. Mowbray, Z. L. Mišković, F. O. Goodman, and Y. N. Wang, Phys. Lett. A **329**, 94 (2004).
[21] D. J. Mowbray, S. Chung, Z. L. Mišković, F. O. Goodman, and Y. N. Wang, Nucl. Instrum. Methods Phys. Res. B **230**, 142 (2005).
[22] D. J. Mowbray, Z. L. Mišković, F. O. Goodman, and Y. N. Wang, Phys. Rev. B **70**, 195418 (2004).
[23] D. J. Mowbray, Z. L. Mišković, and F. O. Goodman, Phys. Rev. B **74**, 195435 (2006).
[24] D. P. Zhou, Y. N. Wang, L. Wei, and Z. L. Miskovic, Phys. Rev. A **72**, 023202 (2005).
[25] D. P. Zhou, Y. H. Song, Y. N. Wang, and Z. L. Miskovic, Phys. Rev. A **73**, 033202 (2006).
[26] M. F. Lin, D. S. Chuu, and W.-K. K. Shung, Phys. Rev. B **56**, 1430 (1997).
[27] M. F. Lin and F. L. Shyu, Phys. Lett. A **259**, 158 (1999).
[28] M. F. Lin and F. L. Shyu, Physica B **292**, 117 (2000).
[29] Y. H. Ho, G. W. Ho, S. C. Chen, J. H. Ho, and M. F. Lin, Phys. Rev. B **76**, 115422 (2007).
[30] O. M. Yevtushenko, G. Ya. Slepyan, S. A. Maksimenko, A. Lakhtakia, and D. A. Romanov, Phys. Rev. Lett. **79**, 1102 (1997).
[31] G. Ya. Slepyan, S. A. Maksimenko, A. Lakhtakia, O. M. Yevtushenko, and A. V. Gusakov, Phys. Rev. B **57**, 9485 (1998).
[32] G. Ya. Slepyan, S. A. Maksimenko, A. Lakhtakia, O. Yevtushenko, and A. V. Gusakov, Phys. Rev. B **60**, 17136 (1999).
[33] R. Saito, M. Fujita, G. Dresselhaus, and M. S. Dresselhaus, Phys. Rev. B **46**, 1804 (1992).
[34] M. F. Lin and W.-K. Kenneth Shung, Phys. Rev. B **52**, 8423 (1995).